New Theory of Flight

Johan Hoffman[*], Johan Jansson[†] and Claes Johnson[‡]

March 28, 2014

Abstract

We present a new mathematical theory explaining the fluid mechanics of subsonic flight, which is fundamentally different from the existing boundary layer-circulation theory by Prandtl-Kutta-Zhukovsky formed 100 year ago. The new theory is based on our new resolution of d'Alembert's paradox showing that slightly viscous bluff body flow can be viewed as zero-drag/lift potential flow modified by 3d rotational slip separation arising from a specific separation instability of potential flow, into turbulent flow with nonzero drag/lift. For a wing this separation mechanism maintains the large lift of potential flow generated at the leading edge at the price of small drag, resulting in a lift to drag quotient of size $15-20$ for a small propeller plane at cruising speed with Reynolds number $Re \approx 10^7$ and a jumbojet at take-off and landing with $Re \approx 10^8$, which allows flight at affordable power. The new mathematical theory is supported by computed turbulent solutions of the Navier-Stokes equations with a slip boundary condition as a model of observed small skin friction of a turbulent boundary layer always arising for $Re > 10^6$, in close accordance with experimental observations over the entire range of angle of attacks including stall using a few millions of mesh points for a full wing-body configuration.

1 Overview of new theory of flight

We present a new theory of flight of airplanes based on computational solution and mathematical analysis of the incompressible Navier-Stokes equations with Reynolds numbers in the range $10^6 - 10^8$ of relevance for small to large airplanes including gliders. The new theory of flight explains how an airplane wing can generate large lift L at small drag D with a lift-to-drag ratio $\frac{L}{D}$ ranging from $15-20$ for a standard wing up to 70 for the long thin wing of an extreme glider, allowing flight at affordable power, which can be viewed as a form of a miracle of real physics.

We show that the flight of an airplane is computable with millions of mesh points, without any need of resolving turbulent boundary layers because their effect of small skin friction shows to be small on main flow characterstics such as lift and drag. By

[*]Professor, School of Computer Science and Communication, KTH, SE-10044 Stockholm, Sweden.
[†]Researcher, School of Computer Science and Communication, KTH, SE-10044 Stockholm, Sweden.
[‡]Professor, School of Computer Science and Communication, KTH, SE-10044 Stockholm, Sweden.

a mathematical stability analysis of computed Navier-Stokes solutions we then show that flight is also understandable.

First outlined in [1, 2] the new theory of flight comes out of our new resolution of d'Alembert's Paradox [3], explaining that zero lift/drag potential flow around a bluff body cannot be observed as a real physical flow, because it is unstable with a specific basic mode of instability arising from opposing flow retardation at stagnation before separation, with *line stagnation* along the trailing edge of a wing associated with a zone of high pressure. This basic mode of instability develops into a quasi-stable separation pattern followed by a turbulent wake, which we describe as *3d rotational slip separation with point stagnation*. Here the high pressure zone of potential flow is replaced by an oscillating pressure with a net suction effect thereby generating drag, and for a wing also lift. We thus find that the flow of air around a wing can be described as *potential flow modified by 3d rotational slip separation with point stagnation*, a large-scale flow which is computationally resolvable except in a turbulent wake where the under-resolution is of little effect for drag and lift.

The new theory shows that the miracle of flight is possible because the flow around a wing: (i) is *incompressible*, and (ii) satisfies a *slip boundary condition* as a model of the small skin friction of the turbulent boundary layer always arising for high Reynolds number. It follows from (i) and (ii) that the flow around a long smooth wing is 2d potential (incompressible, irrotational, stationary and constant in the axial direction) before separation into a turbulent wake, and as such can only separate at *stagnation* with zero flow speed, because (as shown below) the wing section boundary is a streamline. 2d potential flow thus requires a normal pressure gradient to accelerate the flow to follow the upper wing surface directed downwards for a positive *angle of attack* (assuming a symmetric airfoil), see Fig. 1, into what is referred to as *downwash*, which requires low pressure or suction on the upper surface creating about 2/3 of the total lift with 1/3 from high pressure on the lower wing surface. In particular, the flow does not separate on the crest of the wing because there the flow speed is maximal, far from stagnation, and there maximal lift is generated.

Accordingly there is no miracle of flight in moderate or low Reynolds number viscous flow, with a laminar boundary layer satisfying a no-slip boundary condition with zero normal pressure gradient, which separates on the crest without much lift from the upper surface. A small fly cannot glide on fixed wings like a big albatross because the Reynolds number is too small, and has to compensate by very rapid wing flapping.

The new theory makes flight conceptually readily understandable by first recalling that for (horisontal) potential flow around a circular cylinder the pressure drop on top (and bottom) is 3 times the pressure rise in the front (and back) with the flow speed on top twice the incoming speed in accordance with Bernoulli's law. Viewing then a wing as being formed by two circular cylinders of different radii stretching a tube of fabric as shown in Fig. 2, suggests a pressure drop on top about three times the pressure rise up front, which, combined with 3d rotational slip separation without mean pressure rise or drop and with a stretching factor of 3, would give $\frac{L}{D} > 9$. Flight thus shows to be understandable as potential flow modified by 3d rotational slip separation with point stagnation, as illustrated in Fig. 1 showing the generation of large lift on top of the leading edge of potential flow and the separation without mean pressure rise

maintaining large lift at the price of small drag, which can be viewed as a form of *elegant separation*. Large lift thus results from strong suction on the upper part of the leading edge of non-separating potential flow redirecting incoming flow downwards followed by elegant separation without mean pressure rise or drop.

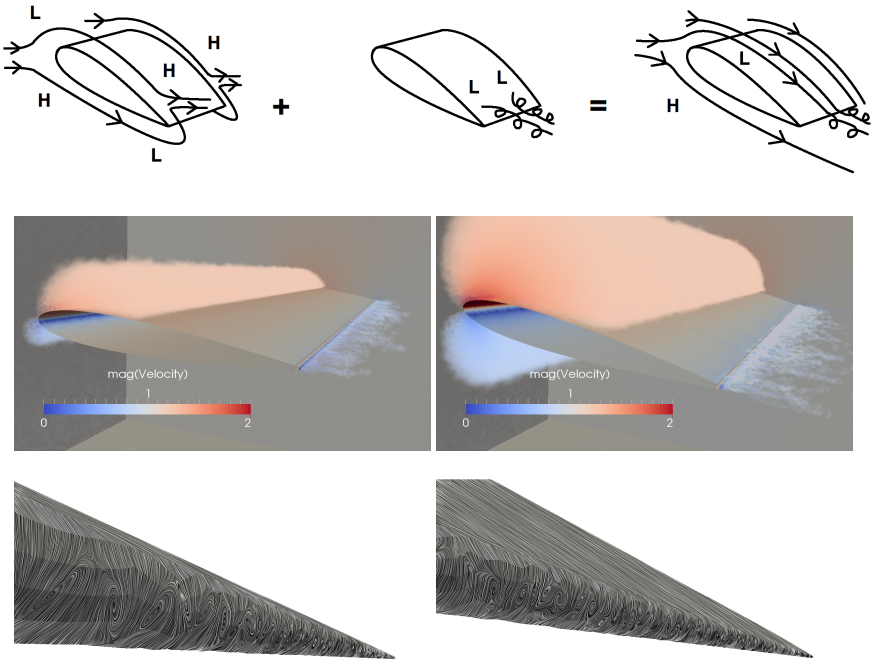

Figure 1: New theory showing potential flow (upper left) being modified at separation by the main instability mode consisting of counter-rotating rolls of streamwise vorticity attaching to the trailing edge (upper middle) to avoid the high pressure buildup at separation which results in a flow with downwash and lift and also drag (upper right), where high (H) and low (L) surface pressure is indicated in the figure. Snapshots of instantaneous flow past a NACA 0012 airfoil at angles of attack 4° (lower left) and 10° (lower right), simulated by computational solution of the Navier-Stokes equations, visualised as magnitude of velocity and limiting streamlines, showing counter-rotating rolls of streamwise vorticity at separation.

In this paper we first highlight differences between the new theory and the classical textbook theory in Section 2, we then present our basic model of subsonic flight in Section 3, which we validate against experimental data in Section 4. In Section 5 we present the basic elements of the new theory, which we summarise in the concluding Section 6 and Section 7.

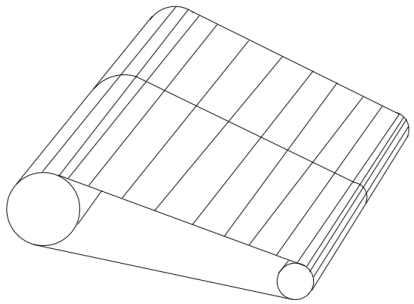

Figure 2: A model of a wing can be constructed by stretching a tube of fabric around two circular cylinders.

2 New theory vs classical textbook theory

The new theory of drag and lift of a wing is fundamentally different from the textbook theory [4, 5, 6, 7, 8, 9, 10, 11, 12, 13] of Prandtl for drag (without lift) based on reduced Navier-Stokes equations in the form of *boundary layer equations with no-slip boundary conditions*, and Kutta-Zhukovsky theory for lift (without drag) of potential flow with slip boundary conditions augumented by a certain amount of large scale *circulation* around the wing section determined by a *Kutta condition* of smooth separation at the trailing edge. This is the *Prandtl-Kutta-Zhukovsky theory* which was developed shortly after powered flight was shown to be possible by the Wright brothers in 1903, breaking the perceived mathematical impossibility of powered flight based on Newton's incorrect theory of lift from air hitting the wing from below. We find that the textbook theory of flight attributed to Prandtl-Kutta-Zhukovsky is incorrect, since it is based on phenomena which are not carried by solutions of the Navier-Stokes equations.

Specifically we find that Prandtl's boundary layer theory with no-slip boundary condition for drag is incorrect, since we combine Navier-Stokes equations with a slip boundary condition modeling the observed small skin friction of high Reynolds number flow, which does not give rise to boundary layers, and yet compute drag in close agreement with experimental observation. We conclude that the main part of the observed drag of a wing does not originate from boundary layers with no-slip boundary conditions.

Further, we find that the Kutta-Zhukovsky theory for lift, based on circulation generated by a sharp trailing edge is incorrect, since we combine Navier-Stokes equations with a rounded trailing edge and yet get lift in close agreement with experimental observation. We conclude that the observed lift of a wing does not originate from a sharp trailing edge as postulated in the Kutta-Zhukovsky theory. On the other hand, we recover the Kutta condition demanding smooth (or elegant) separation at the trailing edge as effectively being realized as 3d rotational slip separation, but without connection to large scale circulation as suggested by Kutta-Zhukovsky.

Although circulation can theoretically generate lift, the logic that since lift is ob-

served there must be circulation, is an example of Aristotle's logical fallacy of confirming the assumption by observing the consequence. In his book *Hydrodynamics* [14] from 1950, the mathematician Garret Birkhoff also questioned [15] Prandtl's boundary layer resolution of d'Alembert's paradox [16], but was criticized in a review by James J. Stoker [17] in strong support of the Prandtl-Kutta-Zhukovsky theory. In fact, as noted e.g. in [18, 19, 20], the generation of circulation has never been given a convincing explanation, and the new theory shows that there is none.

The new theory shows that flight is both computable and understandable and challenges the legacies of Prandtl and Kutta-Zhukovsky, and thereby asks for a complete revision of fundamental parts of textbooks. The state-of-the-art is that computational simulation the flow of air around an airplane to capture lift and drag, requires boundary layer resolution with more than 10^{16} mesh points [21], which would require more than 100 years of Moore's law to be reached. In short, state-of-the-art is that flight is not computable and therefore not understandable: Prandtl tried to explain drag without lift from a very thin no-slip viscous laminar boundary layer, and Kutta-Zhukovsky lift without drag from a slip boundary condition without a boundary layer, but no explanation for lift and drag of real slightly viscous flow with a turbulent boundary layer was given. We show that flight today is computable using millions of mesh points, and understandable as potential flow modified by 3d rotational slip separation, as documented in particular at the AIAA Highlift Workshop 2013 [22].

We hope this paper will result in a constructive discussion including representatives of state-of-the-art flight theory about the central question voiced in the New York Times article *What Does Keep Them Up There?* by Chang from 2003 [23]:

"To those who fear flying, it is probably disconcerting that physicists and aeronautical engineers still passionately debate the fundamental issue underlying this endeavour: what keeps planes in the air?"

3 Mathematical model of subsonic flight

3.1 Navier-Stokes equations

We simulate subsonic flight of an airplane by computational solution of the incompressible *Navier-Stokes equations* in the air volume surrounding the airplane with a combined velocity-stress Dirichlet-Neumann boundary condition on the surface of the airplane prescribing the normal fluid velocity and tangential stress to be zero, with the airplane fixed and the air moving with respect to the coordinate system. This boundary condition is referred to as a *slip condition* valid for an inpenetrable surface with zero friction as an approximation of the observed small skin friction of a turbulent boundary layer at high Reynolds number Re, with $Re \approx 10^6$ for a glider, $Re \approx 10^7$ for a propeller plane at cruising speed and $Re \approx 10^8$ for a jumbojet at take-off and landing, recalling that $Re = \frac{UL}{\nu}$, where U is a charateristic velocity (m/s), L a characteristic length (m) and $\nu \approx 10^{-5}$ is the kinematic viscosity of air (m^2/s).

The Navier-Stokes equations for exterior incompressible flow of (small positive) constant kinematic viscosity ν in a (bounded) volume Ω in $\mathbf{R}^3$ around a fixed rigid body (wing or full wing-body of an airplane) with smooth frictionless boundary Γ (slip

boundary condition) over a time interval $I = [0, T]$, take the following form: Find the velocity $u = (u_1, u_2, u_3)$ and pressure p depending on $(x, t) \in \Omega \cup \Gamma \times I$, such that

$$\begin{aligned} \dot{u} + (u \cdot \nabla)u + \nabla p - \nabla \cdot \tau &= 0 \quad \text{in } \Omega \times I, \\ \nabla \cdot u &= 0 \quad \text{in } \Omega \times I, \\ u_n &= 0 \quad \text{on } \Gamma \times I, \\ \tau_s &= 0 \quad \text{on } \Gamma \times I, \\ u(\cdot, 0) &= u^0 \quad \text{in } \Omega, \end{aligned} \tag{1}$$

where $\dot{u} = \frac{\partial u}{\partial t}$, $u_n = u \cdot n$ is the fluid velocity normal to Γ with n a unit outward normal vector, $\tau = \tau(u) = 2\nu\epsilon(u)$ is the viscous stress with $\epsilon(u)$ the standard velocity strain, τ_s is the tangential stress, u^0 is a given initial condition and we assume suitable far-field inflow/outflow boundary conditions. We focus on high Reynolds number incompressible flow with the slip boundary condition $u_n = 0$ and $\tau_s = 0$ on Γ modeling observed small skin friction, which is instrumental for the generation of $\frac{L}{D}$ larger than 10 required for powered flight. We assume the boundary Γ to be smooth thus eliminating the possibility of attributing lift to a sharp trailing edge, in accordance with the observed fact that lift does not disappear by rounding the trailing edge [24, 25].

We identify a *potential solution* as an incompressible, irrotational and stationary velocity $u = \nabla\phi$ where ϕ is a harmonic function in Ω satisfying a homogeneous Neumann boundary condition on the boundary Γ corresponding to $u_n = 0$, which is an approximate solution of the Navier-Stokes equations (1), together with a corresponding pressure, with a residual scaling with the viscosity ν ($\sim Re^{-1}$) and thus being vanishingly small for vanishing viscosity (increasing Reynolds number). We shall find that potential solutions have fundamental importance because Navier-Stokes solutions at high Re can be viewed as potential solutions modified by 3d rotational slip separation.

3.2 DFS: Weighted residual stabilized finite element method

We compute approximate solutions of the Navier-Stokes equations (1) by a weighted residual stabilized finite element method referred to as Direct Finite Element Simulation DFS, described and analyzed in detail under the acronym G2 as General Galerkin [1]. DFS takes the principal form: Find $\hat{u} = (u, p) \in V_h$ such that for all $\hat{v} = (v, q) \in V_h$

$$[R(u; \hat{u}), \hat{v}] + [hR(u; \hat{u}), R(u; \hat{v})] = 0, \text{for all } \hat{v} \in V_h, \tag{2}$$

where V_h is a space-time finite element space with velocities v satisfying $v \cdot n = 0$ on Γ, $[\cdot, \cdot]$ is an $L_2(\Omega \times I)$ inner product, $R(U; \hat{u}) = (\dot{u} + U \cdot \nabla u + \nabla p, \nabla \cdot u)$ is the residual, and h is the local mesh size. The first term in (2) establishes $\hat{u}$ as a weak solution of (1) and the second term introduces kinetic energy dissipation $[hR(u; \hat{u}), R(u; \hat{u})] = \|h^{0.5}R(u; \hat{u})\|^2_{L_2}$ bounded by data with $\|\cdot\|_{L_2}$ an $L_2(\Omega \times I)$ norm. Basic analysis shows that $\hat{u}$ is an approximate weak solution with residual $R(u; \hat{u})$ in $H^{-1}(\Omega \times I)$ scaling like $h^{0.5}$ [1].

Notice that here ν is set to zero with instead the weighted residual stabilization introducing a dissipative effect as an automatic turbulence model. This is analogous to the dissipative weak solutions introduced by Duchon and Robert [26], with dissipation

caused by a lack of smoothness in the velocity field, unrelated to viscous dissipation. The dissipative effect of a turbulent DFS solution $\hat{u}$ does not disappear when the mesh is refined, instead a Law of finite dissipation is observed where the local dissipation converges to a finite value under mesh refinement [27, 28]. On the other hand, for a smooth solution $\hat{u}$, corresponding to a small residual in $L_2(\Omega \times I)$, the dissipative effect of the weighted residual stabilization vanishes.

3.3 Stability: output error representation by duality

We choose a target output $M(\hat{u}) = [\hat{u}, \hat{\psi}] + [pn, \psi_\Gamma]_\Gamma$, where $\hat{\psi} = (\psi, \chi)$ is a given weight function and ψ_Γ is boundary data for the dual velocity, with $[\cdot,\cdot]_\Gamma$ an $L_2(\Gamma \times I)$ inner product. The difference in output $M(\hat{u}) - M(\hat{U}) = [\hat{u}, \hat{\psi}] + [pn, \psi_\Gamma]_\Gamma - [\hat{U}, \hat{\psi}] - [Pn, \psi_\Gamma]_\Gamma$ of two DFS solutions $\hat{u}$ and $\hat{U}$ on different meshes with maximal mesh size h, can be represented as

$$M(\hat{u}) - M(\hat{U}) = [R(u;\hat{u}) - R(U;\hat{U}), \hat{\varphi}] \tag{3}$$

where $\hat{\varphi} = (\varphi, \theta)$ is a solution of the dual linearized problem

$$\begin{array}{rcll} -\dot{\varphi} - (u\cdot\nabla)\varphi + \nabla U^T\varphi + \nabla\theta &=& \psi & \text{in } \Omega\times I,\\ \nabla\cdot\varphi &=& \chi & \text{in } \Omega\times I,\\ \varphi\cdot n &=& \psi_\Gamma & \text{on } \Gamma\times I,\\ \varphi(\cdot,T) &=& 0 & \text{in } \Omega, \end{array} \tag{4}$$

where $(\nabla U^T\varphi)_j = \sum_{i=1}^3 \partial U_i/\partial x_j \varphi_i$. For example, to choose the lift and drag of an airplane as the target output the dual data is set to $\hat{\psi} = 0$ and $\psi_\Gamma = v_D \cdot n + v_L \cdot n$, with v_D and v_L unit vectors in directions opposite and normal to the flight direction, respectively. Basic analysis shows that (assuming the time step to be bounded by h)

$$|M(\hat{u}) - M(\hat{U})| \le C\|h^{0.5}\hat{\varphi}\|_{H^1}, \tag{5}$$

with a constant C depending on data and bounds on the magnitude of the discrete velocities u and U, and thus establishes stability in output if $\|h^{0.5}\hat{\varphi}\|_{H^1}$ is small [1].

To construct an adaptive algorithm we compute a DFS solution $\hat{U}$ for which we use the error representation (3) to estimate the output error $|M(\hat{u}) - M(\hat{U})|$, with $\hat{u}$ any DFS solution computed on a finer mesh than $\hat{U}$. If the estimated error is too large the mesh is locally refined to increase the precision in $M(\hat{U})$. The adaptive mesh refinement algorithm is based on an estimate of the local contribution to the global error, which is obtained by splitting the error representation (3) into a sum of *error indicators* $\mathcal{E}_{n,K}$ over the discrete space mesh $\mathcal{T}^h$ and time intervals $I_n = (t_{n-1}, t_n)$, $n = 1, ..., N$, that is

$$M(\hat{u}) - M(\hat{U}) = \sum_{n=1}^N \sum_{K\in\mathcal{T}^h} \mathcal{E}_{n,K} = \sum_{n=1}^N \sum_{K\in\mathcal{T}^h} [R(u;\hat{u}) - R(U;\hat{U}), \hat{\varphi}]_{n,K} \tag{6}$$

with $[\cdot,\cdot]_{n,K}$ an $L_2(K\times I_n)$ inner product. The error representation (6) can be the basis for a number of different adaptive algorithms based on optimization of the mesh and

the finite element space V_h. One basic adaptive algorithm is to keep the mesh constant in time and then iteratively refine the spatial mesh based on (6) until convergence in $M(\hat{U})$ is observed. If the estimated global error in (6) is within the tolerance, the adaptive algorithm is terminated.

There are several technical aspects with respect to how to apply the error representation formula (6), in particular with regards to the approximation of $\hat{\varphi}$, the solution to the dual problem. The dual problem is linear, but runs backward in time which is a challenge since the DFS solutions $\hat{u}$ and $\hat{U}$ act as coefficients in the dual problem and thus have to be stored as data. In practise, the dual problem is solved using a similar finite element method as for the primal DFS problem, and the coefficients $\hat{u}$ and $\hat{U}$ can be interpolated in time to minimize data storage. The function $\hat{u}$ can be taken as a DFS solution on a different mesh in the adaptively generated hierarchy of meshes, or be an ideal function representing a finest possible resolution with $M(\hat{u})$ the target value for the output approximation $M(\hat{U})$, where we then use the approximation $\hat{u} \approx \hat{U}$ in the dual problem. Also, several different approaches are possible for how to apply the error representation formula (3) in practise, to retain sharpness and achieve maximal robustness, see e.g. [29].

For simple geometries high Reynolds number bluff body flow has been investigated in detail [1, 30, 31, 32, 33, 28], where it is found that a computed DFS solution shows to have small residual (of order $h^{0.5}$) in the weak norm of $H^{-1}(\Omega \times I)$, and to be *turbulent* in the wake identified by locally large residual (order $h^{-0.5}$) in the stronger $L_2(\Omega \times I)$-norm [27]. Combined with observed boundedness in $H^1(\Omega \times I)$ of the dual solution (weighted by $h^{-0.5}$), we find computational evidence that errors in lift and drag on the level of a few percent can be reached with a few hundred thousands mesh points for simple geometries. The observed boundedness in the weighted $H^1(\Omega)$ norm of the dual solution, with distributed input data for lift and drag output, can be understood as an effect of cancellation from a highly oscillating reaction coefficient ∇u in the wake.

3.4 DFS of subsonic flight

We compute DFS solutions of (1) for a long wing and a wing-body configuration, choosing lift and drag as mean value output quantities with corresponding data in the associated dual problem, and with adaptive mesh refinement geared by the error representation (3). The flow shows to be computationally resolvable except in a wake behind the wing, as potential flow modified by 3d rotational slip separation into a turbulent wake stretching out into the farfield behind the airplane, see Fig. 4. Computed solutions show the pressure distribution on the body surface with lift L and drag D obtained by integration of the surface pressure. The computed results are in close agreement with experimental observations for a long NACA 0012 wing with maximal $\frac{L}{D} \approx 50$, and for a complete wing-body configuration with $\frac{L}{D} \approx 20$ over the entire range of angle attack from zero to beyond stall [34, 22].

A computed partly turbulent solution displays a large scale resolvable quasi-stable flow except in a not fully resolved turbulent wake. The computational resolution of the turbulent wake shows to have little influence on the pressure distribution on the body and thus on lift and drag, which is supported by the nature of the dual solution

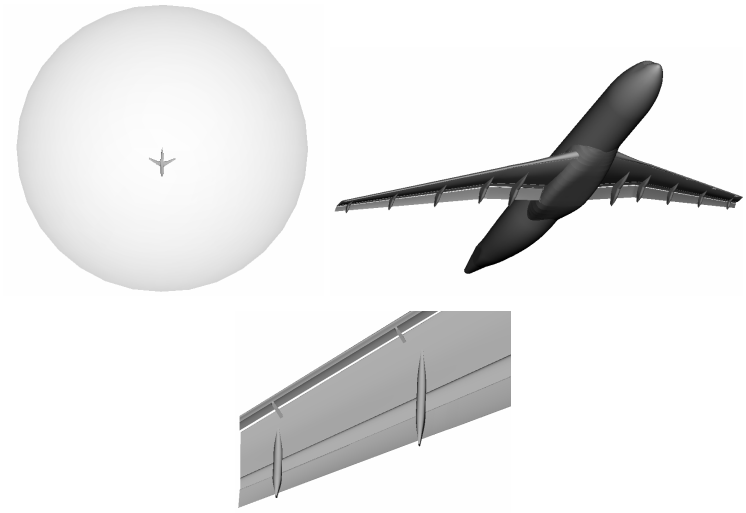

Figure 3: Overview of the computational domain Ω for the DLR-F11 aircraft model (upper) and detail of wing pressure side (lower). On the detail snapshot of the wing pressure side, *slat tracks* and *flap fairings* are seen.

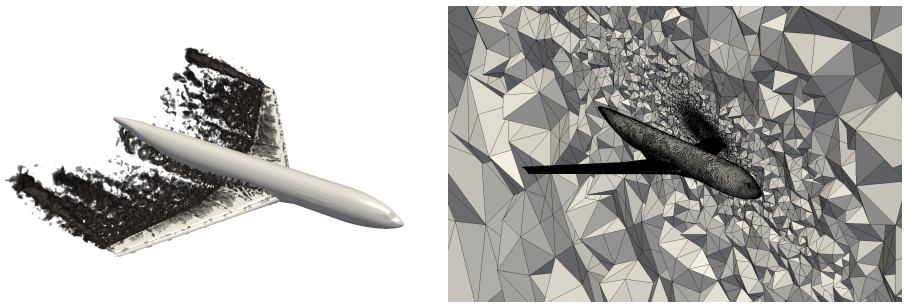

Figure 4: Snapshot of a DFS solution of the flow around of a wing-body configuration with vorticity visualised by a Q-criterion (left), with an adaptively refined computational mesh optimised for lift and drag approximation [22].

displayed in Fig. 5 with little weight in the wake. A computed solution can thus be viewed as a representative resolved Navier-Stokes solution with small residual in the weak global norm of $H^{-1}(\Omega \times I)$ in accordance with [35], and locally small residual in the strong norm of $L_2(\Omega \times I)$, except in a turbulent wake with large residual in $L_2(\Omega \times I)$, with wake under-resolution of little impact on surface pressure distribution, lift and drag.

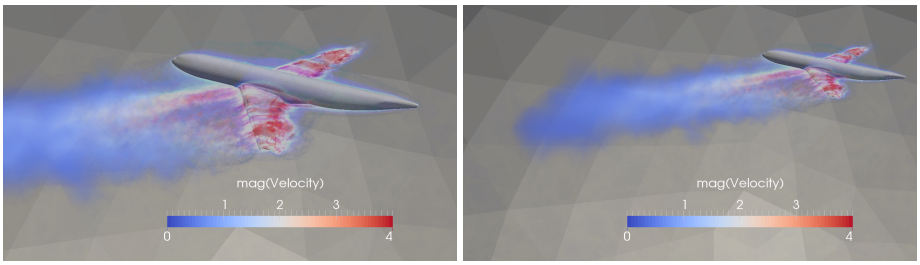

Figure 5: Snapshot of the solution of the dual linearised Navier-Stokes equations with data corresponding to the output quantities lift and drag on the wing-body configuration. We note the magnitude of the dual solution which is small in the downstream wake [22].

DFS/G2 is extensively documented and validated with experiments [36, 1, 30, 31, 32, 33, 34, 37, 38, 39, 40, 22] and can for high Reynolds number flow be viewed as a parameter-free model since the weight in the residual stabilization is set equal to the local mesh size of a finite element mesh (without small angles). The effect of mesh refinement is resolution of the near-field around the wing-body, see Fig. 4, with further resolution concentrating on the far-field wake with little impact on lift and drag. Lift and drag thus show to be computable within a few percent using a couple of hundred thousands of mesh points in simple geometry and millions in complex geometry.

G2/DFS is the first methodology based on the full time-dependent Navier-Stokes equations capable of simulating high Reynolds number bluff body flow in complex geometry, without model or parameter input from the user. We note that G2/DFS can be used with non-zero skin friction, and also with boundary layer resolution using no-slip boundary conditions although at a much higher cost which effectively prevents simulation of high Reynolds number flow. In [41, 42, 34, 37, 39, 40, 22] we give computational evidence that for $Re > 10^7$ the skin friction is so small that it can be put to zero as a slip boundary condition without noticeable effect on lift and drag.

3.5 The Clay Navier-Stokes Millennium Problem

The fact that a computed solution is partly turbulent with locally large residual in $L_2(\Omega \times I)$, can be seen as evidence of non-existence of a well-posed smooth solution to the Navier-Stokes equations with smooth data, in the case of small viscosity bluff body flow, and thus as a negative answer to the Clay Navier-Stokes Millennium Problem [43], which unfortunately does not contain the fundamental aspect of well-posedness identified by Hadamard [44]: For bluff body flow, physically meaningful well-posed

solutions are non-smooth even if data is smooth, and globally smooth solutions are not well-posed.

4 Validation of the computational model

In the previous section we introduced the Navier-Stokes equations with slip boundary condition as the basic mathematical model of subsonic flight, with G2/DFS as a methodology to compute solutions to the mathematical model. The purpose of this section is to present a validation of the model (1) by comparing DFS computational results with experimental data in two examples related to flight. The first example is the NACA 0012 wing [34] which is a standard test case, and the second example is a full wing-body configuration used as benchmark in the AIAA HighLift workshop [22].

4.1 Long NACA 0012 wing

We model the flow around a wing in a virtual wind tunnel. The computational setup is a wind tunnel with square cross-section 2.7×2.7 meters (m) and of length 5.32 m, in which we place a NACA 0012 wing with a chord length of 0.76 m. On the tunnel walls we use free slip boundary conditions, at the inlet we set a constant inflow $U = 1ms^{-1}$, and at the outlet we use zero stress outflow boundary conditions [1]. At the wing surface we use zero skin friction boundary conditions, corresponding to a free slip boundary condition, modelling the small skin friction of high Reynolds number flow.

For a set of angles of attack α, DFS simulations are performed over the time interval $I = [0, 10]$, where for each angle of attack the computational mesh is adaptively refined based on a posteriori estimation of the error in mean total force on the wing (both drag and lift) until convergence, over the time interval $I_m = [5, 10]$ (where the flow is assumed to be fully developed). Results from DFS reported in [34] show lift and drag in close agreement with experimental measurements [46, 45], see Fig. 6. The corresponding surface pressure distributions for a pre-stalled angle of attack is shown in Fig. 7, also close to experimental data.

The experimental measurements are performed at high Reynolds numbers, but still significantly lower than in the case of a real aircraft. One effect of a lower Reynolds number is the development of laminar separation bubbles at the leading edge of the wing at high angles of attack, which causes a decrease in lift [46]:

"...it might be that an intermediate range of Reynolds numbers exists over which the section exhibits a combined leading-edge and trailing-edge type stall. This implies that above some Reynolds number within the range of the tests, the aerofoil starts to stall with turbulent-boundary-layer separation moving forward from the trailing edge, but the flow breakdown is completed by an existing laminar separation of the flow in the leading-edge region failing to re-attach. At some higher Reynolds number, however, transition from laminar to turbulent flow would be expected to precede laminar separation so that the stall would then be entirely controlled by the forward movement of turbulent separation."

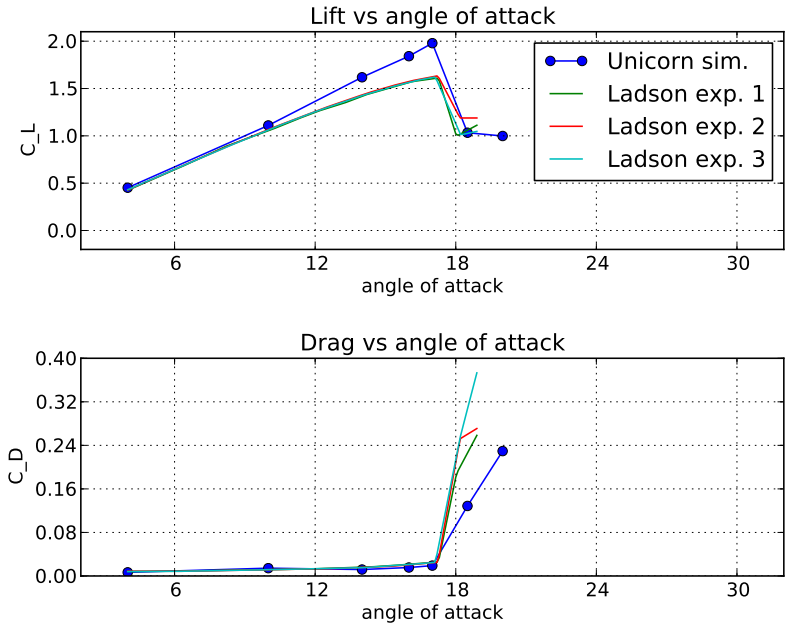

Figure 6: Lift and drag coefficients from DFS for a NACA 0012 wing plotted against the angle of attack, together with experimental results from Ladson [45].

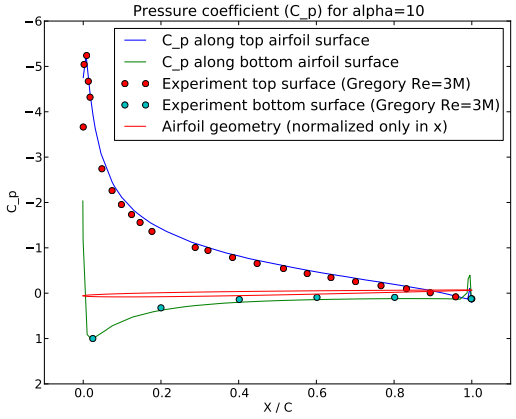

Figure 7: G2 computation of pressure coefficient for a NACA 0012 wing, averaged in time and in the spanwise direction, along the lower and upper parts of the wing for an angle of attack 10°. Note in particular the low pressures near the trailing edge of the wing corresponding to suction from the attached flow over the rounded trailing edge.

In [46] it is reported that a laminar separation bubble is present from roughly angle of attack 9°, which coincides with an observed flattening of the lift curve [46, 45]. Since the DFS simulation is an idealisation of an infinite Reynolds number no laminar separation bubbles develop, and thus lift is higher than in the experiments for high angles of attack, and likely also closer to the real case of a an aircraft at higher Reynolds numbers where turbulent boundary layers are fully developed.

4.2 Complete wing-body

Next we report results from the 2013 AIAA CFD High Lift Prediction Workshop [47], where DFS was used to simulate the time-dependent flow past a full wing-body configuration [22]. The DFS solver was the only fully time-dependent Navier-Stokes solver in the workshop, and no other methodology (such as RANS [48]) showed better agreement with experimental observation, even at much higher computational cost (in terms of the number of degrees of freedom). Free slip boundary conditions (zero skin friction) was used in the DFS model to simulate the low skin friction of high Reynolds number flow, and the mesh was adaptively refined based on a posteriori estimation of the error in lift and drag.

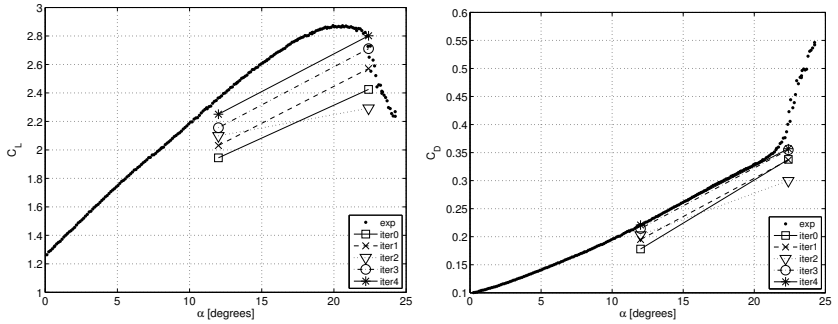

Figure 8: Lift and drag coefficient for angles of attack 12° and 22.4°, under adaptive mesh refinement with the computational approximations approaching the experimental reference values.

Simulations were performed for a number of angles of attack, from attached flow through partly separated flow to stall. We find that for angles of attack corresponding to a pre-stalled flow, DFS simulation captures the lift and drag in experiments within a few percent, see Fig. 8. For a stalled aircraft the computed lift is also close to experiments, while the error in drag is somewhat larger. The local surface pressure over the wing is well approximated in the DFS computation, see Fig. 9-10. Under adaptive mesh refinement the lift and drag approach the experimental reference values [22], and with additional mesh refinement the precision is expected to increase further.

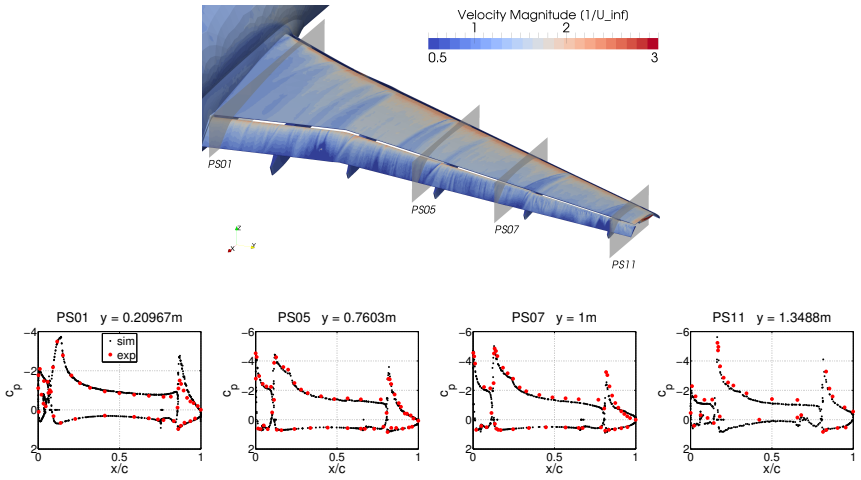

Figure 9: Mean velocity contours and measurement plane locations (upper), and pressure coefficient, C_P, vs. normalized local chord, x/c, (lower) for the angle of attack $\alpha = 12^o$, for a complete wing-body configuration.

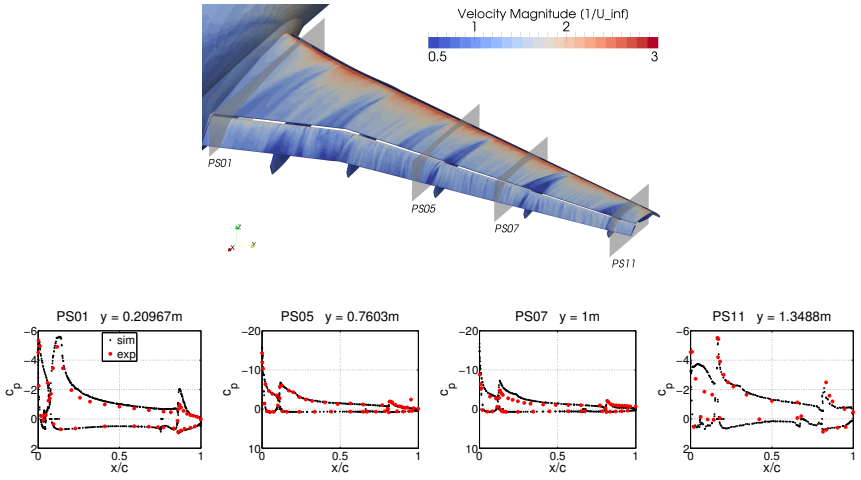

Figure 10: Mean velocity contours and measurement plane locations (upper), and pressure coefficient, C_P, vs. normalized local chord, x/c, (lower) for the angle of attack $\alpha = 22.4^o$, for a complete wing-body configuration.

5 Elements of the new theory of flight

We now present the key elements of the new theory of flight, in the form of the drag and lift generated by a wing. Contrary to the classical theory which is based on 2d potential flow, effects from a vanishingly thin boundary layer, and an infinitely sharp trailing edge, we construct the new theory directly from the fundamental model (1) of 3d flow past a smooth wing. To model the flow around a wing we start from the circular cylinder, for which we analyse the stability of flow attachment and separation.

5.1 From circular cylinder to wing

Experimental studies of the flow past a circular cylinder under increasing Reynolds number shows a sudden drop in drag at $Re \approx 10^5 - 10^6$ referred to as *drag crisis*, which is a consequence of delayed separation due to transition to turbulence in the boundary layer, into the development of a pattern of streamwise vortices for $Re > 10^6$ that we refer to as 3d rotational slip separation [49, 50, 51, 52, 53].

G2/DFS simulations exhibit this scenario under decreasing skin friction towards free slip at the boundary, as a model of a turbulent boundary layer under increasing Reynolds number, with close agreement in drag compared with experiments [42]. As we refine the mesh we find that that the large scale features of the flow around the cylinder including separation pattern, surface pressure and drag, change little under decreasing mesh size. The effect of mesh refinement downstream the cylinder is an extension of the length of the turbulent wake, as shown in Fig. 11 .

The flow around a circular cylinder can be used as a model of both leading edge attachment and rounded trailing edge separation for a long wing viewed as two circular cylinders joined by two sheets, see Fig. 2. We now analyse the stability of potential flow as an approximate solution of (1), where we find that 3d rotational slip separation is realized as a quasi-stable flow with minimal retardation by point stagnation and with oscillating high and low pressure, to be compared with unstable 2d irrotational potential flow separation from line stagnation with high pressure. We start with the following observation:

Theorem 1: *Two-dimensional potential flow in a domain Ω exterior to a wing section with smooth boundary Γ, can only separate at a stagnation point with zero flow velocity*.
Proof: Let the potential flow velocity $u = \nabla\phi$ with ϕ a harmonic function and let ψ be the corresponding conjugate function. The level lines of ϕ and ψ are orthogonal, with the boundary Γ a level line of ψ wherever $u = \nabla\phi$ is bounded away from zero. Fluid particles close to Γ follow streamlines as level lines of ψ which are parallel to the boundary Γ wherever $u = \nabla\phi$ is bounded away from zero, because level lines of ϕ are orthogonal to Γ. Fluid particles thus cannot separate from the boundary as long as $u = \nabla\phi$ is bounded away from zero. □

In particular, it follows that potential flow around a long wing cannot separate on the crest of the wing, because there the flow velocity cannot vanish. The slip condition satisfied by potential flow is thus instrumental for the generation of lift. We note that 2d potential flow past a wing section with smooth boundary must have a stagnation point

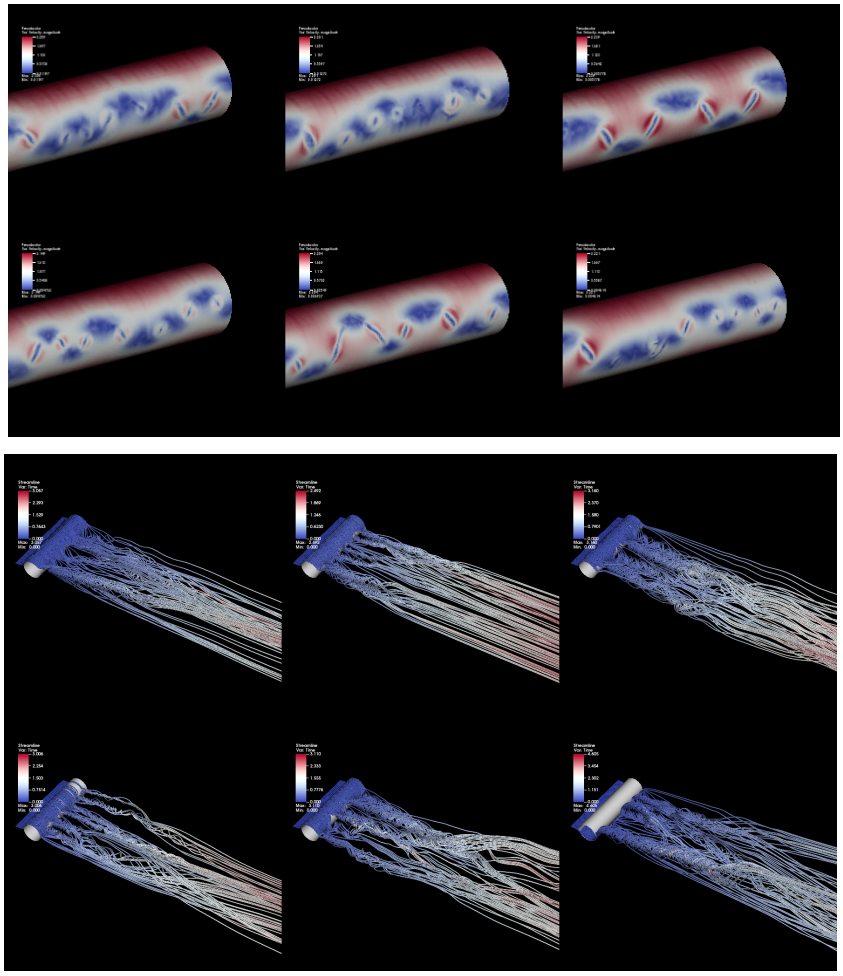

Figure 11: Snapshots of velocity magnitude (upper) and streamlines (lower) illustrating the quasi-static large scale flow features which are stable under mesh refinement. The figure displays the solution after 13, 15, 17, 19, 21 and 23 adaptive mesh refinements with respect to the error in drag [42].

at the trailing edge from meeting opposing flow coming from above and below the section. Potential flow past a long wing thus necessarily separates with line stagnation and thus the basic instability necessarily appears, as the origin of stable lift and drag making controlled flight possible.

5.2 Potential flow

Potential flow around a long circular cylinder, of unit radius with axis along the x_3-axis in $\mathbf{R}^3$ with coordinates $x = (x_1, x_2, x_3)$, assuming the flow velocity is $(1, 0, 0)$ at infinity in each x_2x_3-plane, is given by the following potential in polar coordinates (r, θ) in a plane orthogonal to the cylinder axis, see Fig. 12:

$$\varphi(r,\theta) = (r + \frac{1}{r})\cos(\theta)$$

with corresponding velocity components

$$u_r \equiv \frac{\partial\varphi}{\partial r} = (1 - \frac{1}{r^2})\cos(\theta), \quad u_s \equiv \frac{1}{r}\frac{\partial\varphi}{\partial\theta} = -(1 + \frac{1}{r^2})\sin(\theta)$$

and with streamlines being level lines of the conjugate potential function

$$\psi \equiv (r - \frac{1}{r})\sin(\theta).$$

Potential flow is constant in the direction of the cylinder axis with velocity $(u_r, u_s) = (1, 0)$ for r large, is fully symmetric with zero drag/lift, attaches and separates at the lines of stagnation $(r, \theta) = (1, \pi)$ in the front and $(r, \theta) = (1, 0)$ in the back. By Bernouilli's principle the pressure is given by

$$p = -\frac{1}{2r^4} + \frac{1}{r^2}\cos(2\theta)$$

when normalized to vanish at infinity. We compute

$$\frac{\partial p}{\partial\theta} = -\frac{2}{r^2}\sin(2\theta), \quad \frac{\partial p}{\partial r} = \frac{2}{r^3}(\frac{1}{r^2} - \cos(2\theta)),$$

and discover an adverse pressure gradient in the back. We shall now see that the potential flow around a circular cylinder shows exponentially unstable 2d irrotational separation and quasi-stable 2d attachment, and is a useful model for both attachment at the leading edge of a wing and separation at a rounded trailing edge.

5.3 Linearized Navier-Stokes equations with vanishing viscosity

We analyze the stability of a potential solution as a smooth solution of the Navier-Stokes equations (1) with vanishing viscosity and skin friction through the linearized Euler equations

$$\begin{array}{rcll} \dot{v} + (u\cdot\nabla)v + (v\cdot\nabla)\bar{u} + \nabla q &=& f - \bar{f} & \text{in } \Omega\times I,\\ \nabla\cdot v &=& 0 & \text{in } \Omega\times I,\\ v\cdot n &=& 0 & \text{on } \Gamma\times I,\\ v(\cdot,0) &=& u^0 - \bar{u}^0 & \text{in } \Omega, \end{array} \tag{7}$$

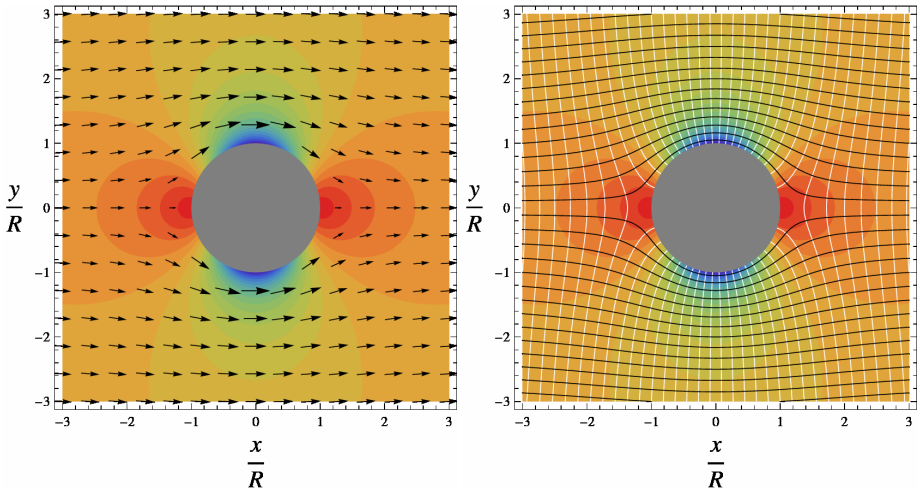

Figure 12: Potential flow around circular cylinder: colormap of pressure, velocity field (left), velocity potential and stream function (right).

where (u, p) and $(\bar{u}, \bar{p})$ are two Euler solutions with slightly different initial data (u^0 and $\bar{u}^0$) and volume forcing (f and $\bar{f}$), and we denote the difference by $(v, q) \equiv (u - \bar{u}, p - \bar{p})$. Formally, with u and $\bar{u}$ given, this is a linear convection-reaction problem for (v, q) with growth properties governed by the reaction term given by the 3×3 matrix $\nabla\bar{u}$. By the incompressiblity, the trace of $\nabla\bar{u}$ is zero, which shows that in general $\nabla\bar{u}$ has eigenvalues with real values of both signs, of the size of $|\nabla u|$ (with $|\cdot|$ some matrix norm), thus with at least one exponentially unstable eigenvalue, except in the neutrally stable case with purely imaginary eigenvalues, or in the non-normal case of degenerate eigenvalues representing parallel shear flow [1].

The linearized equations in velocity-pressure indicate that, as an effect of the reaction term $(v \cdot \nabla)\bar{u}$:

- streamwise retardation is exponentially unstable in velocity,
- transversal acceleration is neutrally stable,

where transversal signifies a direction orthogonal to the flow direction.

5.4 The vorticity equation

Additional stability information is obtained by applying the curl operator $\nabla\times$ to the momentum equation $\dot{u} + (u \cdot \nabla)u + \nabla p = f$ with forcing f viewed as a perturbation of the zero forcing in (1), to give the *vorticity equation*

$$\dot{\omega} + (u \cdot \nabla)\omega - (\omega \cdot \nabla)u = \nabla \times f \quad \text{in } \Omega, \tag{8}$$

which is also a convection-reaction equation in the *vorticity* $\omega = \nabla\times u$ with coefficients depending on u, of the same form as the linearized equations (7), with a sign change of

the reaction term. The vorticity is thus also locally subject to exponential growth with exponent $|\nabla u|$:

- streamwise acceleration is exponentially unstable in streamwise vorticity (vortex stretching).

It thus seems possible that vorticity may grow large from a small force perturbation f with $\nabla \times f$ less small, and this is what we see in computer simulations. This means that *Kelvin's theorem*, often cited in fluid dynamics textbooks, stating that vorticity without forcing will remain zero if it is zero initially and at inflow, as a consequence of the vorticity equation (8) with $\nabla \times f = 0$ and $u_n = 0$ on Γ, is a result which is not stable under small perturbations and as such is not well-posed in Hadamard's sense and thus is not a result about physical flow. Viewing Kelvin's theorem as a result about real flow, as is often done, is thus based on a misconception. In particular, Kutta and Zhukovsky made the world believe that a wing must have a sharp trailing edge, since the circulation they needed to get lift could not result from anything but a singularity defying Kelvin's theorem.

We shall now exhibit in more detail how 3d rotational slip separation, as the basic mode of instability in 2d irrotational potential flow separation, can develop from the exponential instability in streamwise retardation identified in (7) followed by vortex stretching in acceleration identified in (8). We thus give evidence that the possibilty of instability, so obvious by the presence of the reaction terms with coefficient ∇u in (7) and (8), can be made into a reality of turbulence, recalling that it is turbulence which allows a wing to generate stable lift and drag.

5.5 Exponential instability of 2d irrotational separation

We identify the basic instability mechanism at separation of 2d potential flow around a circular cylinder resulting from opposing retarding flow with line stagnation connected to high pressure, which creates a quasi-stable large-scale flow with minimal retardation and oscillating surface pressure in a pattern of point stagnation, which we describe as 3d rotational slip separation. We find that the flow has large scale resolvable features except in a turbulent wake where under-resolution shows to have little impact on lift and drag.

To analyze the stability of 2d irrotational separation we use potential flow in a half-plane as a model of trailing edge separation: $u(x) = (x_1, -x_2, 0)$ in the half-plane $\{x_1 > 0\}$ with stagnation along the line $(0, 0, x_3)$ and

$$\frac{\partial u_1}{\partial x_1} = 1 \quad \text{and} \quad \frac{\partial u_2}{\partial x_2} = -1, \tag{9}$$

expressing that the fluid is *squeezed* by *retardation* in the x_2-direction and *acceleration* in the x_1-direction. We first focus on the retardation with the main stability feature of (7) captured in the following simplified version of the v_2-equation of (7), assuming x_1 and x_2 are small,

$$\dot{v}_2 - v_2 = f_2,$$

where we assume $f_2 = f_2(x_3)$ to be an oscillating perturbation depending on x_3 of a certain wave length δ and amplitude h, for example $f_2(x_3) = h\sin(2\pi x_3/\delta)$, expecting the amplitude to decrease with the wave length. We find, assuming $v_2(0,x) = 0$, that

$$v_2(t,x_3) = (\exp(t) - 1)f_2(x_3).$$

We next turn to the accelleration and then focus on the ω_1-vorticity equation, for x_2 small and $x_1 \geq \bar{x}_1 > 0$ with $\bar{x}_1$ small, approximated by

$$\dot{\omega}_1 + x_1\frac{\partial\omega_1}{\partial x_1} - \omega_1 = 0,$$

with the "inflow boundary condition"

$$\omega_1(\bar{x}_1,x_2,x_3) = \frac{\partial v_2}{\partial x_3} = (\exp(t) - 1)\frac{\partial f_2}{\partial x_3}.$$

The equation for ω_1 thus exhibits exponential growth, which is combined with exponential growth of the "inflow condition". We can see these features in principle and in computational simulation in Fig. 13 showing how opposing flows at separation generate a pattern of alternating surface vortices from pushes of fluid up/down, which act as initial conditions for vortex stretching into the fluid generating counter-rotating low-pressure tubes of streamwise vorticity.

The above model study can be extended to the full linearized equations linearized at $u(x) = (x_1, -x_2, 0)$:

$$\begin{aligned} Dv_1 + v_1 &= -\tfrac{\partial q}{\partial x_1}, \\ Dv_2 - v_2 &= -\tfrac{\partial q}{\partial x_2} + f_2(x_3), \\ Dv_3 &= -\tfrac{\partial q}{\partial x_3}, \\ \nabla\cdot v &= 0, \end{aligned} \tag{10}$$

where $Dv = \dot{v} + u\cdot\nabla v$ is the convective derivative with velocity u and $f_2(x_3)$ as before. We here need to show that the force perturbation $f_2(x_3)$ will not get cancelled by the pressure term $-\frac{\partial q}{\partial x_2}$ in which case the exponential growth of v_2 would get cancelled. The force perturbation $f_2(x_3)$ will induce a variation of v_2 in the x_3 direction, but this variation does not upset the incompressibility since it does not involve the variation in x_2. Thus, there is no reason for the pressure q to compensate for the force perturbation f_2 and thus exponential growth of v_2 is secured.

5.6 3d rotational slip separation for circular cylinder

We thus discover streamwise vorticity generated by a force perturbation oscillating in the x_3 direction, which in the retardation of the flow in the x_2-direction creates exponentially increasing vorticity in the x_1-direction, which acts as inflow to the ω_1-vorticity equation with exponential growth by vortex stretching. That is, we find exponential growth at rear separation in both the retardation in the x_2-direction and the acceleration in the x_1-direction, as a result of the squeezing expressed by (9).

The corresponding pressure perturbation changes the high pressure at separation of potential flow into a zig-zag alternating quasi-stable pattern of moderate pressure variations with elevated pressure zones deviating opposing flow into non-opposing streaks which are captured by low pressure zones to form rolls of streamwise vorticity allowing the flow to spiral away from the body. This scenario is similar to the vortex formed in a bathtub drain.

The larger the scale of the vortices, the more stable is the rotational separation, since unstable streamwise retardation can be minimized. The most stable configuration of the zig-zag pattern of vortices is thus the one corresponding to the maximal size of the vortices allowed by the geometry with minimal retardation. At start-up from zero velocity, streamwise vorticity in computer simulations is triggered from perturbations on the same scale as the mesh size, which is rapidly modified into mesh independent large scale streamwise vortices of the same scale as the geometry. We shall see that the tubes of low-pressure streamwise vorticity change the normal pressure gradient to allow separation without unstable retardation, but the price is generation of drag by elimination of the high pressure of zero drag potential flow as a "cost of separation". We have now identified *3d rotational slip separation* as one of two crucial parts of the miracle of flight, the other being potential flow with slip boundary condition.

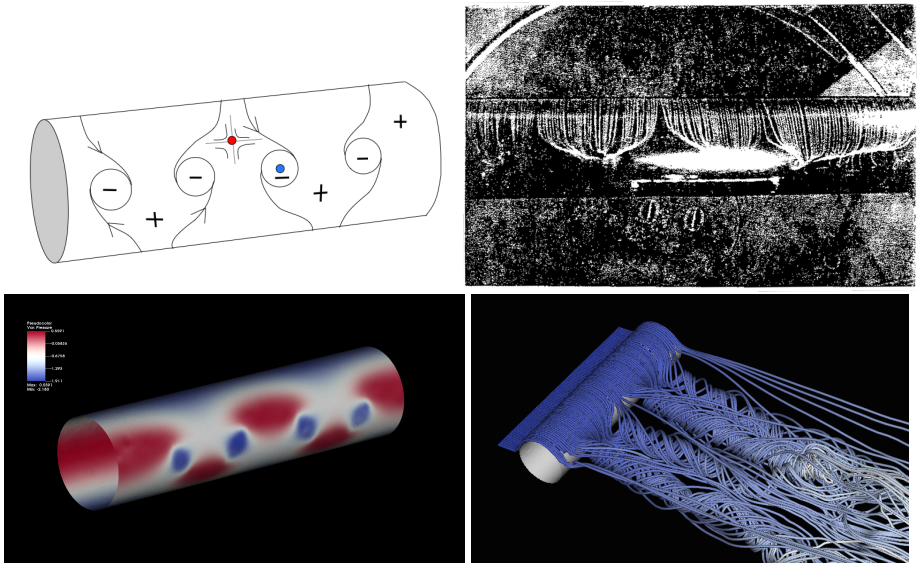

Figure 13: Illustration of quasi-stable separation pattern with point stagnation for a circular cylinder (upper left), and observed in experiment using silk threads attached at the upstream attachment line [50] (upper right), with corresponding computer simulation [42] showing surface pressures (lower left) and velocity streamlines (lower right).

5.7 Quasi-stable 3d rotational slip separation

As a model of 3d rotational slip separation at $x = (0, 0, 0)$ into the halfplane $x_1 > 0$, we consider $u(x) = (2\epsilon x_1, x_3 - \epsilon x_2, -x_2 - \epsilon x_3)$ with the corresponding linearized equations

$$\dot{v}_1 = -2\epsilon v_1, \quad \dot{v}_2 + v_3 = \epsilon v_2, \quad \dot{v}_3 - v_2 = \epsilon v_3, \tag{11}$$

where $\epsilon \geq 0$. With $\epsilon = 0$, the flow $u(x)$ represents rotating flow with neutrally stable transversal acceleration. With $\epsilon > 0$ the flow $u(x)$ is retarding in x_2 (and x_3), but in this case a perturbation $f_2(x_3)$ will be affected by the rotation preventing the instability of 2d irrotational separation. We thus find analytical evidence the computationally observed quasi-stability of 3d rotational slip separation, connecting to the observed stability of the rotating flow through a bathtube drain emerging from the instability of non-rotating radially symmetric and retarding drain flow.

Further, the surface pattern of 3d rotational slip separation given in Fig. 13 shows high pressure stagnation points as 2d saddle points in the plane $x_1 = 0$ of the form $(0, -x_2, x_3)$, to be compared with the unstable flow $(x_1, -x_2, 0)$ analyzed above (as well as stable stagnation points inside low pressure rotational flow). The analog to the unstable perturbation $f_2(x_3)$ for $(x_1, -x_2, 0)$, would be a perturbation $f_2(x_1)$ potentially generating transversal vorticty in the x_3 direction, which however would be blocked by the surface (similar to that in attachment) and also be subject to destruction by the main flow in the x_1 direction away from the surface.

The observed quasi-stability of the surface flow of 3d rotational slip separation including 2d saddle points depicted in Fig. 13, thus can be understood from a linearized stability analysis, an essential aspect being the different stability properties of $(x_1, -x_2, 0)$ and $(0, -x_2, x_3)$ with the main flow in the x_1-direction, which we record as a basic fact in

Theorem 2: *The saddle point flow $u(x) = (x_1, -x_2, 0)$ is stable in the plane $x_3 = 0$, but unstable in the half space $x_1 > 0$.*

Proof: We have already proved instability in the half-space $x_1 > 0$ as the origin of 3d rotational slip sepration, and we thus consider the 2d case in the plane $x_3 = 0$. Fluid particles follow trajectories $(x_1(t), x_2(t))$ as solutions of $\dot{x}_1 = x_1$, $\dot{x}_2 = -x_2$, while the linearized equations in velocity perturbations (v_1, v_2) take the form $\dot{v}_1 = -v_1$, $\dot{v}_2 = v_2$. Exponential growth/decay along a fluid particle trajectory is thus balanced by exponential decay/growth in perturbation, with the effect that the velocity perturbation v_2 which is subject to exponential growth will be initialized as a perturbation of an exponentially small particle velocity u_2, without the possibility of a substantial oscillating perturbation $f_2(x_3)$ as in the case $x_1 > 0$, with the effect that exponential growth and decay cancel under restriction to $x_3 = 0$, and stability follows. □

5.8 Quasi-stable potential flow attachment

The above analysis also shows that potential flow attachment, even though it involves streamwise retardation, is quasi-stable. This is because the initial perturbation f_2 in the above analysis is forced to be zero by the slip boundary condition requiring the normal velocity to vanish. In short, potential flow attachment is stable because the flow is retarded by the solid body and not by opposing flows as in separation.

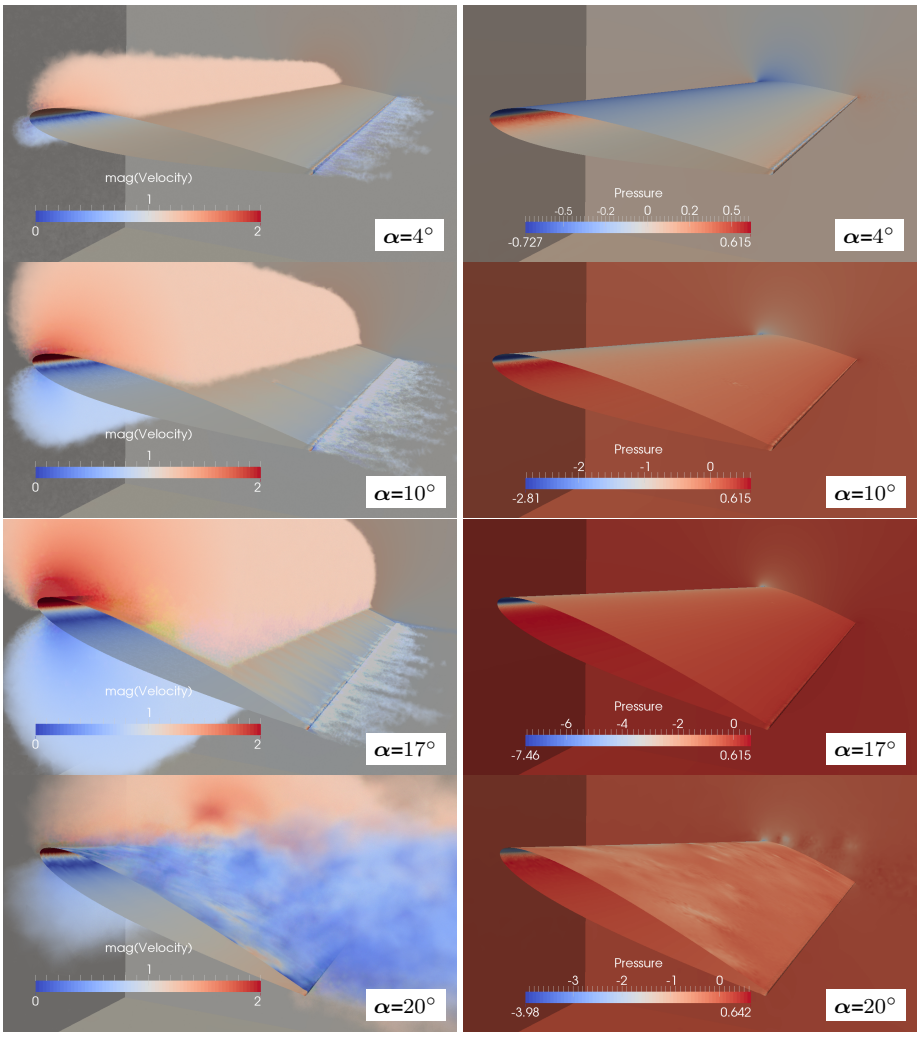

Figure 14: Flow around NACA 0012 wing under increasing angle of attack, illustrated by plots of the magnitude of the velocity (left) and surface pressure (right).

5.9 Practical consequence: rounded trailing edge

In the classical Kutta-Zhukovsky circulation theory there is no lift without a sharp trailing edge. The impact of this theory on practice is seen in the UIUC Airfoil Coordinate Database [54] which lists 1550 airfoils, all with sharp trailing edge, despite early experiments [24, 25] showing that a rounded edge of diameter less than 1% of the chord length gives essentially the same lift and drag as a maximally sharp edge, while a moderate increase of drag was noted for 2%.

The new theory assumes that the trailing edge is more or less smoothly rounded, which opens to both mathematical analysis and computation, and also fits with practice: in general real wings do not have knife-sharp trailing edges, with up to 10% rounding of modern wind turbine wings with improved stall characteristics.

5.10 Lift and drag invariance from scale invariance

The Navier-Stokes equations with slip and vanishingly small viscosity are scale invariant in the sense that a change of the scale in space leaves the equations invariant. We therefore expect the 3d rotational separation pattern at the trailing edge including the pressure variation on the trailing edge surface to remain the same with total effect tending to zero with the radius of the trailing edge. We may thus expect lift and drag to vary little for small radii of the trailing edge, which is also observed experimentally [24, 25].

As the radius tends to zero the wake flow can be described as a complex "vortex sheet" of counter-rotating rolls of streamwise vorticity with the length increasing with decreasing viscosity (increasing Reynolds number), analogous to what we see in simulations when the computational mesh is refined, see Fig. 11.

6 Descriptive scenario for different angles of attack

The elements of the new theory are now collected into a description of the flow around a long wing, e.g. formed by stretching a fabric between two cylinders, as potential flow modified by 3d rotational slip separation at a smoothly rounded trailing edge as illustrated in Fig. 1-2.

By Theorem 1 the flow being 2d potential cannot separate from the upper part of the wing before stall, and therefore is redirected downwards, which requires low pressure on the upper surface creating lift which is kept by 3d rotational separation without the mean pressure rise of 2d irrotational potential flow separation cancelling lift.

We now give a detailed description of the flow pattern for different angles of attack α, exemplified by the NACA 0012 wing, see Fig. 6. Altogether, we see lift increasing linearly with the angle of attack as a consequence of redirection into downwash until stall for $\alpha > 17$, drag staying nearly constant for $\alpha < 14$ as a consequence of unchanging separation pattern, with only weak linear increase due to an increasing effective thickness of the wing (projection in the flow direction) with the separation moving up on the trailing edge onto the upper surface, and finally quickly increasing

drag under beginning stall for $14 < \alpha < 17$ with separation on the upper surface, after which the wing essentially behaves as a bluff body, see Fig. 14.

7 Summary of New Theory of Flight

The new theory shows that the miracle of flight is made possible by the combined effects of (i) incompressibility, (ii) slip boundary condition and (iii) 3d rotational slip separation, creating a flow around a wing which can be described as (iv) potential flow modified by 3d rotational separation. The basic novelty of the theory is expressed in (iii) as a fundamental 3d flow phenomenon only recently discovered by advanced computation and analyzed mathematically, and thus is not present in the classical theory. Finally, (iv) can be viewed as a realization in our computer age of Euler's original dream to in his equations capture an unified theory of fluid flow.

The crucial conditions of (ii) a slip boundary condition and (iii) 3d rotational slip separation show to be safely satisfied by incompressible flow if the Reynolds number is larger than 10^6. For lower Reynolds numbers the new theory suggests analysis and design with focus on maintaining (ii) and (iii).

Acknowledgements

The authors would like to thank our collaborators Niclas Jansson and Rodrigo Vilela De Abreu who generously contributed images from [42, 34, 22].

The authors also acknowledge the financial support from the Swedish Foundation for Strategic Research, the European Research Council, and the Swedish Research Council. The simulations were performed on resources provided by the Swedish National Infrastructure for Computing (SNIC) at PDC – Center for High-Performance Computing. The authors also thankfully acknowledges the computer resources, technical expertise and assistance provided by the Red Española de Supercomputacion and the Barcelona Supercomputing Center - Centro Nacional de Supercomputacion.

The initial volume mesh in [22] was generated with ANSA from Beta-CAE Systems S. A., who generously provided an academic license for the project.

References

[1] J. Hoffman and C. Johnson, Computational Turbulent Incompressible Flow, Springer 2007.

[2] J. Hoffman and C. Johnson, Mathematical Secret of Flight, Normat, Vol.57, pp.145-169, 2009.

[3] J. Hoffman and C. Johnson, Resolution of d'Alembert's paradox, J. Math. Fluid Mech., Vol.12(3), pp.321-334, 2010.

[4] T. von Karman and W. R. Sears, Airfoil theory for non-uniform motion, AIAA Journal. Vol. 41, no. 7A, pp. 5-16. 2003.

[5] D. A. Peters, S. Karunamoorthy and W.-M. Cao, Finite state induced models part 1: two-dimensional thin airfoil, AIAA Journal of Aircraft, Vol. 32(2), 1995.

[6] Prandtl, Essentials of Fluid Mechanics, Herbert Oertel (Ed.), 2004.

[7] Introduction to the Aerodynamics of Flight, Theodore A. Talay, Langley Reserach Center, 1975.

[8] Aerodynamics of the Airpoplane, Hermann Schlichting and Erich Truckenbrodt,Mac Graw Hill, 1979.

[9] Fundamentals of Aerodynamics, John D Anderson, 2010.

[10] Aerodynamics, Aeronautics and Flight Mechanics, McCormick, 1995.

[11] Aerodynamics, Krasnov, 1978.

[12] Aerodynamics, von Karmann, 2004.

[13] Theory of Flight, Richard von Mises, 1959.

[14] G. Birkhoff, Hydrodynamics: a study in logic, fact, and similitude, 1950.

[15] Garret Birkhoff in Hydrodynamics, 1950: *I think that to attribute dAlemberts paradox to the neglect of viscosity is an unwarranted oversimplification. The root lies deeper, in lack of precisely that deductive rigour whose importance is so commonly minimised by physicists and engineers*.

[16] L. Prandtl, On Motion of Fluids with Very Little Viscosity, Third International Congress of Mathematics, Heidelberg, 1904.

[17] J. Stoker in Review of [14] in Bull. Amer. Math. Soc. 57 (6): 497499:*On the other hand, the uninitiated would be very likely to get wrong ideas about some of the important and useful achievements in hydrodynamics from reading this chapter.In the case of air foil theory, for example, the author treats only the negative aspects of the theory. It has always seemed to the reviewer that the Kutta-Joukowsky theory of airfoils is one of the most beauti- ful and striking accomplishments in applied mathematics. The fact that the introduction of a sharp trailing edge makes possible a physi- cal argument, based on consideration of the effect of viscosity, that leads to a purely mathematical assumption regarding the behavior of an analytic function which in its turn makes the solution to the flow problem unique and also at the same time furnishes a value for the lift force, represents a real triumph of mathematical ingenuity.*

[18] David Bloor, The Enigma of the Aerofoil: Rival Theories in Aerodynamics, 1909-1930, The University of Chicago Press, 2011.

[19] J. Hoffren, Quest for an improved explanation of lift, AIAA 2001-0872, 39th AIAA Aerospace Sciences Meeting and Exhibit, Reno, 2001.

[20] J. Hoffren, Quest for an Improved Explanation of Lift, AIAA Journal 2001:*The classical explanations of lift involving potential flow, circulation and Kutta conditions are criticized as abstract, non-physical and difficult to comprehend. The basic physical principles tend to be buried and replaced by mystical jargon...Classical explanations for the generation of lift do not make the essence of the subject clear, relying heavily on cryptical terminology and theorems from mathematics. Many classical texts even appear to have a fundamental error in their underlying assumptions...Although the subject of lift is old, it is felt that a satisfactory general but easily understandable explanation for the phenomenon (of lift), is still lacking, and consequently there is a genuine need for one.*

[21] J. Kim and P. Moin, Tackling Turbulence with Supercomputer, Scientific American.

[22] J. Hoffman, J. Jansson, N. Jansson and R. Vilela De Abreu, Time-resolved adaptive FEM simulation of the DLR-F11 aircraft model at high Reynolds number, Proc. 52nd Aerospace Sciences Meeting, AIAA, 2014.

[23] Kenneth Chang; Staying Aloft: What keeps them up there?, New York Times, Dec 9, 2003.

[24] J. Stack, W. F. Lindsay, NACA Technical Report 665, 1938.

[25] L. Joseph Herrig, James C. Emery and John R. Erwin, Effects of Section Thickness and Trailing-Edge Radius on TBE Performance of NAAC 65smms Compressor Blades in Cascade, NACA Research Memorandum L51J16, 1956.

[26] J. Duchon and R. Robert, Inertial energy dissipation for weak solutions of incompressible Euler and Navier-Stokes equations, Nonlinearity, Vol.13, pp.249-255, 2000.

[27] J. Hoffman and C. Johnson, Blowup of Euler solutions, BIT Numerical Mathematics, Vol 48, No 2, 285-307, 2008.

[28] J. Hoffman, J. Jansson and R. Vilela De Abreu, Adaptive modeling of turbulent flow with residual based turbulent kinetic energy dissipation, Comput. Meth. Appl. Mech. Engrg., Vol.200(37-40), pp.2758-2767, 2011.

[29] W. Bangerth and R. Rannacher, Adaptive finite element methods for differential equations, Springer, 2003.

[30] J. Hoffman, C. Johnson, A new approach to computational turbulence modeling, Comput. Methods Appl. Mech. Engrg. 195 (2006) 2865–2880.

[31] J. Hoffman, Adaptive simulation of the turbulent flow past a sphere, J. Fluid Mech., 568 (2006), pp. 77–88.

[32] J. Hoffman, Computation of mean drag for bluff body problems using adaptive dns/les, SIAM J. Sci. Comput., 27(1) (2005), pp. 184–207.

[33] J. Hoffman, Efficient computation of mean drag for the subcritical flow past a circular cylinder using general galerkin g2, Int. J. Numer. Meth. Fluids, 59(11) (2009), pp. 1241–1258.

[34] J.Jansson, J.Hoffman and N.Jansson, Simulation of 3D flow past a NACA 0012 wing section, in review (available as CTL technical report kth-ctl-4023).

[35] J. Leray, Sur le mouvement d'un liquide visqueux emplissant l'espace, Acta Mathematica, Vol.63, pp.193-248, 1934.

[36] J. HOFFMAN, J. JANSSON, R. VILELA DE ABREU, C. DEGIRMENCI, N. JANSSON, K. MÜLLER, M. NAZAROV AND J. HIROMI SPÜHLER, *Unicorn: parallel adaptive finite element simulation of turbulent flow and fluid-structure interaction for deforming domains and complex geometry*, Computers and Fluids, Vol.80, pp.310-319, 2013.

[37] R. Vilela De Abreu, N. Jansson and J. Hoffman, Adaptive computation of aeroacoustic sources for rudimentary landing gear, in proceedings for Workshop on Benchmark problems for Airframe Noise Computations I, Stockholm, 2010.

[38] N. Jansson, J. Hoffman, M. Nazarov, Adaptive Simulation of Turbulent Flow Past a Full Car Model, in: Proceedings of the 2011 ACM/IEEE International Conference for High Performance Computing, Networking, Storage and Analysis, SC '11, 2011.

[39] R. Vilela de Abreu, N. Jansson and J. Hoffman, Computation of Aeroacoustic Sources for a Complex Landing Gear Geometry Using Adaptive FEM, Proceedings for the Second Workshop on Benchmark Problems for Airframe Noise Computations (BANC-II), Colorado Springs, 2012.

[40] R.Vilela de Abreu, N.Jansson and J.Hoffman, Adaptive computation of aeroacoustic sources for rudimentary landing gear, Int. J. Numer. Meth. Fluids, Vol., Vol.74(6), pp.406-421, 2014.

[41] J.Hoffman, Simulation of turbulent flow past bluff bodies on coarse meshes using General Galerkin methods: drag crisis and turbulent Euler solutions, Comp. Mech. 38 pp.390-402, 2006.

[42] J. Hoffman and N. Jansson, A computational study of turbulent flow separation for a circular cylinder using skin friction boundary conditions, in proceedings for Quality and Reliability of Large-Eddy Simulations II, Pisa, Italy, 2009.

[43] C. L. Fefferman, Official clay prize problem description: Existence and smoothness of the navier-stokes equation, 2000.

[44] J. Hadamard, Sur les problémes aux dérivées partielles et leur signification physique. Princeton University Bulletin, pp. 4952, 1902.

[45] C. Ladson, U. S. N. Aeronautics, S. A. Scientific, T. I. Division, Effects of independent variation of Mach and Reynolds numbers on the low-speed aerodynamic characteristics of the NACA 0012 airfoil section, NASA technical memorandum, National Aeronautics and Space Administration, Scientific and Technical Information Division, 1988.

[46] N. Gregory, C. C.L. O'Reilly, Low-speed aerodynamic characteristics of NACA 0012 aerofoil section, including the effects of upper-surface roughness simulating hoar frost, Aeronautical Research Council (Great Britain), Reports and memoranda, H.M.S.O., 1973.

[47] Rumsey, C., 2nd AIAA CFD High Lift Prediction Workshop HiLiftPW-2, (http://hiliftpw.larc.nasa.gov/), 2013.

[48] P. Sagaut, Large Eddy Simulation for Incompressible Flows (3rd Ed.), Springer-Verlag, Berlin, Heidelberg, New York, 2005.

[49] M. M. Zdravkovich, Flow around circular cylinders: a comprehensive guide through flow phenomena, experiments, applications, mathematical models, and simulations. Vol.1 [Fundamentals], Oxford Univ. Press, Oxford, 1997.

[50] A. I. Korotkin, The three dimensionality of the flow transverse to a circular cylinder, Fluid Mechanics - Soviet Research, Vol.5, 1976.

[51] J. S. Humphreys, On a circular cylinder in a steady wind at transition Reynolds numbers, Journal of Fluid Mechanics, Vol.9(4), pp.603-612, 1960.

[52] G. Schewe, Reynolds-number effects in flow around more or less bluff bodies, 4 Intern. Colloquium Bluff Body Aerodynamics and Applications, also in Journ. Wind Eng. Ind. Aerodyn. 89 (2001).

[53] B. Gölling, Experimentelle Untersuchungen des laminar-turbulenten Ueberganges der Zylindergrenzschichtströmung, DLR, 2001.

[54] UIUC Airfoil Data Site, http://www.ae.illinois.edu/m-selig/ads.html